SCIENCE CHINA
Technological Sciences

• Article •

July 2024 Vol. 67 No. 7: 2191–2202
https://doi.org/10.1007/s11431-023-2651-6

Distributed swarm control for multi-robot systems inspired by shepherding behaviors

SUN GuiBin[1], GU HaiBo[1,2] & LÜ JinHu[1,2*]

[1] *School of Automation Science and Electrical Engineering, Beihang University, Beijing* 100191*, China;*
[2] *Zhongguancun Laboratory, Beijing* 100094*, China*

Received December 9, 2023; accepted March 26, 2024; published online June 25, 2024

Swarming behaviors play an eminent role in both biological and engineering research, and show great potential applications in many emerging fields. Traditional swarming models still lack integrity, uniformity, and stability in swarm forming processes, resulting in fragmentation and void phenomena. Inspired by the shepherding behaviors observed in nature, we propose an integrated negotiation-control scheme for distributed swarm control of massive robots. The core idea of this scheme is that the robots at the boundary of the group herd the internal robots to form an equilibrium swarm. For this purpose, we introduce a concept of virtual group center towards which boundary robots herd internal robots. Then, a distributed negotiation mechanism is designed to allow each robot to negotiate the virtual group center only through local interactions with its neighbors. After that, we propose a shepherding-inspired swarm control law to drive a group of robots to form an integrated, uniform, and stable configuration from any initial states. Both numerical and flight simulations are presented to verify the effectiveness of our proposed swarm control scheme.

swarm control, multi-robot system, negotiation-control scheme, shepherding behavior

Citation: Sun G B, Gu H B, Lü J H. Distributed swarm control for multi-robot systems inspired by shepherding behaviors. Sci China Tech Sci, 2024, 67: 2191–2202, https://doi.org/10.1007/s11431-023-2651-6

1 Introduction

In nature, groups of biological swarms can emerge various collective behaviors that are functional for swarms adapting to the environment and survive [1, 2]. These fascinating behaviors provide valuable insights into building massive multi-robot collaboration systems. This study focuses on the problem of distributed swarm control that has received tremendous attention in recent years due to its great potential across many domains [3–10]. The objective of swarm control is to steer a group of robots to assemble an equilibrium configuration from any initial disorder states in a distributed manner. Swarm control is important for robots to achieve desired navigation tasks or dynamically respond to the environment.

Significant progress in swarm control is to develop simple models by simulating the internal mechanisms of natural swarming behaviors [11]. Most of the existing works rely on the Reynolds framework [12], i.e., repulsion in the short range, velocity alignment in the middle range, and attraction in the long range. On the basis of these primary rules, researchers have developed hundreds of models to implement synchronized collective motion of multi-robot systems, such as Vicsek model [13–15], Couzin model [16–18], Cucker-Smale model [19–21], and Olfati model [22, 23]. These models can be called self-organized because the interactions between robots are completely local and the motion decisions are made independently by the robots themselves [14].

Self-organization is an important characteristic of swarm systems [24]. In motion decision-making, robots require considering not only their states, but also the behaviors of other neighboring robots. In social creatures, limited by the ability

*Corresponding author (email: jhlu@iss.ac.cn)

to acquire information, such consideration is a local observation, that is, each robot only perceives neighbors' states [25, 26]. As for artificial swarms, such as multi-robot systems, since the support of wireless technology, information can be shared between robots. Therefore, this consideration can be a broader global observation, which would be conducive to robots making more reasonable decisions and avoiding falling into local optimal [27]. However, most of the existing approaches rarely consider global behavior with a broader perspective. Although these methods can realize swarm intelligence to a certain extent, due to the lack of global observation, local minimum may occur, such as fragmentation and void phenomena which are well-known pitfalls of swarm control [22]. The work in ref. [22] solves these problems by informing all the robots of a time-varying reference to be tracked, which is not fully distributed.

Motivated by the above analysis, this study focuses on the problem of fully distributed swarm control of multi-robot systems considering the global observation. This problem has rarely been addressed in existing studies. The studies in ref. [28] proposed a control algorithm to maintain the connectivity of the swarm network by introducing the group center. Here, the group center, whose calculation requires a centralized approach, is inherently global information. Instead, Gu and Wang [29] presented a decentralized consensus protocol to estimate the group center via local interactions. These two works can be regarded as typical methods of considering the global information. Subsequently, Bhowmick et al. [30] improved the estimation protocol of the group center. However, the difference between the estimated group center and the actual group center is still large. In addition, these methods [28–30] only consider the single-integrator model due to its simplicity. However, this model usually cannot well approximate real robot dynamics well because the velocity of a single integrator can be arbitrarily assigned [31].

Despite the existing approaches, the following challenges remain open to overcome. The most important thing is how to prevent robot swarms from falling into a local minimum using only local peer-to-peer information. Since the local measurement, it is difficult to obtain the global stabilization to the group center. The second problem is the accuracy of group center negotiation in local information environments. Existing methods can provide the convergence of the negotiation protocol, but cannot accurately estimate the group center. Thus, it is still an open problem whether robots can reach a consensus on the group center with only local interactions.

Compared with the existing results, the novelty and contribution of this paper are summarized as threefold. First, we establish an integrated negotiation-control swarm scheme to avoid local optimal problems such as fragmentation and void phenomena. The key component to resolve this is the virtual group center (inherently global information), which is obtained through local negotiations among robots. It is called a "virtual group center" because it is not the actual center of the robot swarm yet a consensus center negotiated by all the robots. Such a negotiation-control scheme has been employed in our previous work on the shape formation of swarm robots [32]. In contrast, we here consider a more complex case of the double-integrator model. Second, we propose a distributed negotiation protocol to address the negotiation problem on the virtual group center in both free swarm control and time-varying swarm control. Compared with the existing methods [28–30], we provide a guarantee that our proposed negotiation protocol can converge to the desired states globally and asymptotically. Third, we propose a shepherding-inspired swarm control strategy for massive robots. Here, we introduce two types of robots with different roles, i.e., herding robots acting as shepherd dogs and herded robots acting as sheep. The core idea of this strategy is that herding robots control herded robots to form an equilibrium swarm. The comparison between our strategy and two state-of-the-art methods [11, 22] demonstrates the improvement of integrity, uniformity, and stability for swarm control.

2 Problem statement

Consider a group of n autonomous robots in $\mathbb{R}^d$, where $n \geqslant 2$ and $d = 2$ or 3. Each robot is regarded as a circle with the body size of r_b, and it can interact with other robots within the sensing range of r_s. Without loss of generality, we can use a double integrator to describe the motion of each robot:

$$\begin{cases} \dot{\boldsymbol{p}}_i = \boldsymbol{v}_i, \\ \dot{\boldsymbol{v}}_i = \boldsymbol{u}_i, \end{cases} \quad (i = 1, \ldots, n), \tag{1}$$

where $\boldsymbol{p}_i, \boldsymbol{v}_i, \boldsymbol{u}_i \in \mathbb{R}^d$ represent the position, velocity, and acceleration command of robot i, respectively. The double-integrator model is closer to the actual system than the single integrator. In practice, the control and planning of quadrotors can be designed based on a double integrator [33, 34].

The interaction among robots is described by an undirected graph $\mathcal{G} = (\mathcal{V}, \mathcal{E})$, which consists of a vertex set $\mathcal{V} = \{1, ..., n\}$ and an edge set $\mathcal{E} \subseteq \mathcal{V} \times \mathcal{V}$ such that

$$\mathcal{E} = \left\{(i, j) : \left(\boldsymbol{p}_i, \boldsymbol{p}_j\right) \in \mathcal{D}, i, j \in \mathcal{V}, j \neq i\right\}$$

with $\mathcal{D} = \{(\boldsymbol{p}_i, \boldsymbol{p}_j) \in \mathbb{R}^d \times \mathbb{R}^d : \|\boldsymbol{p}_i - \boldsymbol{p}_j\| < r_s\}$, where $\|\cdot\|$ refers to the Euclidean norm in $\mathbb{R}^d$. The edge $(i, j) \in \mathcal{E}$ indicates that robot i can receive information from robot j, and robot j is a neighbor of robot i. Thus, the set of neighbors of robot i is

$$\mathcal{N}_i = \left\{j \in \mathcal{V} : \left(\boldsymbol{p}_i, \boldsymbol{p}_j\right) \in \mathcal{D}\right\}. \tag{2}$$

In refs. [22, 32], to simplify the problem analysis, it is often assumed that robots can perceive neighboring individuals within a certain distance, which is called a metric interaction topology.

The objective of this paper is to steer a group of robots from their initial disorder configuration to assemble an integrated, uniform, and stable spatial structure in such a way that the herding robots enclose the remaining herded robots (Figure 1). Different from shape formation problems where robots can form user-specified shapes [35–37], we here allow robots to spontaneously form a certain shape configuration only relying on local interactions with their neighbors, also known as swarm aggregation [38]. To do that, robots first need to reach an agreement on virtual group center with their neighbors, as shown in Figure 1(b). At the same time, the herding robots at the boundary of the group control the herded robots inside the group to form an equilibrium configuration, as shown in Figure 1(c). One may notice that the role of each robot is dynamically switched according to the robot's location in the group. Furthermore, the swarm robots should be able to track a time-varying reference while maintaining the equilibrium configuration. Next, we show how to design an appropriate swarm control scheme to achieve such an objective.

3 Distributed negotiation on virtual center

The proposed swarm control scheme consists of two components, as shown in Figure 1(a). The first is a distributed negotiation protocol that can autonomously reach a consensus among robots on the final location of the virtual group center. The second is a swarm control strategy that drives swarm robots to form an equilibrium configuration by imitating the process of shepherding sheep. This section first addresses how to design the distributed negotiation protocol.

3.1 Negotiation protocol design

Our scheme is to allow robots to reach a consensus on the final location of the virtual group center. While one may specify the coordinate of the virtual group center by informing all robots, we here consider a fully distributed scenario where each robot negotiates and finally reaches a consensus on the virtual group center in a distributed manner (Figure 1(b)).

Let $\boldsymbol{p}_{\mathrm{c}}$ and $\boldsymbol{v}_{\mathrm{c}}$ be the position and velocity vectors of the virtual group center, respectively. The interpretations of $\boldsymbol{p}_{\mathrm{c}}$ and $\boldsymbol{v}_{\mathrm{c}}$ by robot i are denoted as $\hat{\boldsymbol{p}}_{\mathrm{c},i}$ and $\hat{\boldsymbol{v}}_{\mathrm{c},i}$. Then, the interpretations of all the robots on the virtual group center can reach an agreement by the following negotiation protocol:

$$\dot{\hat{\boldsymbol{v}}}_{\mathrm{c},i} = -\sum_{j\in\mathcal{N}_i} a_{ij}\left[c_1\left(\hat{\boldsymbol{p}}_{\mathrm{c},i}-\hat{\boldsymbol{p}}_{\mathrm{c},j}\right)+c_2\left(\hat{\boldsymbol{v}}_{\mathrm{c},i}-\hat{\boldsymbol{v}}_{\mathrm{c},j}\right)\right]-\hat{\boldsymbol{v}}_{\mathrm{c},i}, \tag{3}$$

where constant $c_1 > 0$ and variable $c_2 = \alpha_1 + c_1/(\alpha_1\gamma_i)$. Here, α_1 is a positive constant, and γ_i satisfies $\gamma_i = \sum_{j\in\mathcal{N}_i} a_{ij}$. The adjacency coefficient $a_{ij} \in \{0, 1\}$ is determined by: if $j \in \mathcal{N}_i$, $a_{ij} = 1$, and otherwise $a_{ij} = 0$. Initially, $\hat{\boldsymbol{p}}_{\mathrm{c},i}(t_0) = \boldsymbol{p}_i(t_0)$ and $\hat{\boldsymbol{v}}_{\mathrm{c},i}(t_0) = 0$ show that each robot treats itself as a statically virtual group center. The convergence analysis of eq. (3) under this initial condition will be presented later in Theorem 1.

As can be seen from eq. (3), the first term is the state coordination component. Its primary objective is to reduce the negotiation deviation of neighboring robots for the virtual group center and ensure that the state interpretations can converge uniformly in the end. The second term is a damping velocity, whose responsibility is to adjust the evolution speed of the virtual group center.

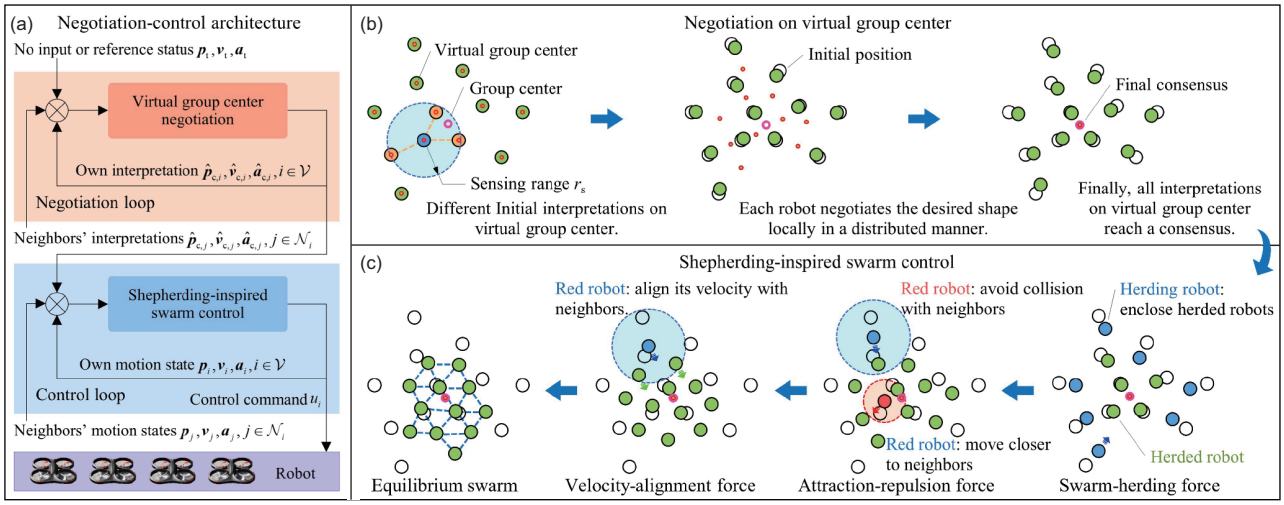

Figure 1 An overview of the integrated negotiation-control swarm scheme. (a) Architecture of the proposed scheme. (b) Example to show the negotiation process of robots. (c) Example to show the swarm control process of robots.

Next, we present the convergence analysis of the proposed negotiation protocol (eq. (3)). To do that, we make the following assumptions.

Assumption 1 The negotiation process converges faster than the control process.

This assumption is valid because the negotiation process is a numerical computational process that relies only on virtual states, that is, $\hat{\boldsymbol{p}}_{\mathrm{c},i}$ and $\hat{\boldsymbol{v}}_{\mathrm{c},i}$. These states are not subject to the physical dynamics of the robot. In contrast, the control process is subject to the real physical dynamics of the robot. As a result, the control process evolves much slower. The subsequent simulation results support this assumption.

Assumption 2 The swarm network $\mathcal{G}$ remains connected and time-invariant.

Network connectivity is the basis for the global convergence of swarm control algorithms [39,40]. Assumption 2 is valid when the initial graph is connected and Assumption 1 is valid. Specifically, when the negotiation process converges, the swarm configuration is almost unchanged and thus $\mathcal{G}$ remains connected and time-invariant. In fact, an alternative that can strictly ensure the assumption of $\mathcal{G}$ would be to run an initialization process, during which we wait for the negotiation process to converge first.

Then, we discuss the nonsingularity of γ_i by Lemma 1 and show the convergence of protocol (eq. (3)) by Theorem 1.

Lemma 1 Under Assumption 2, $\gamma_i > 0$ for all $i \in \mathcal{V}$.

Proof. Recall that $\gamma_i = \sum_{j\in\mathcal{N}_i} a_{ij}$. Since all the diagonal entries of degree matrix $\boldsymbol{D}(\mathcal{G})$ is positive by Assumption 2, it holds that $\gamma_i > 0$ for all $i \in \mathcal{V}$.

Theorem 1 At the initial moment, let $\hat{\boldsymbol{p}}_{\mathrm{c},i}(t_0) = \boldsymbol{p}_i(t_0)$ and $\hat{\boldsymbol{v}}_{\mathrm{c},i}(t_0) = 0$ for all $i \in \mathcal{V}$. Under Assumption 2, the position interpretations under protocol (eq. (3)) converge to the means of all the robots' initial interpretations globally and asymptotically.

Proof. Suppose $\hat{\boldsymbol{p}}_{\mathrm{c}} = [\hat{\boldsymbol{p}}_{\mathrm{c},1}^{\mathrm{T}}, ..., \hat{\boldsymbol{p}}_{\mathrm{c},n}^{\mathrm{T}}]^{\mathrm{T}}, \hat{\boldsymbol{v}}_{\mathrm{c}} = [\hat{\boldsymbol{v}}_{\mathrm{c},1}^{\mathrm{T}}, ..., \hat{\boldsymbol{v}}_{\mathrm{c},n}^{\mathrm{T}}]^{\mathrm{T}} \in \mathbb{R}^{dn}$. The matrix-vector form of eq. (3) is

$$\dot{\hat{\boldsymbol{v}}}_{\mathrm{c}} = -c_1\tilde{\boldsymbol{L}}\hat{\boldsymbol{p}}_{\mathrm{c}} - c_2\tilde{\boldsymbol{L}}\hat{\boldsymbol{v}}_{\mathrm{c}} - \hat{\boldsymbol{v}}_{\mathrm{c}}, \tag{4}$$

where $c_1, c_2 > 0$ and $\tilde{\boldsymbol{L}} = \boldsymbol{L} \otimes \boldsymbol{I}_d$. Here, $\boldsymbol{I}_d \in \mathbb{R}^{d\times d}$ is an identity matrix, and $\boldsymbol{L}$ is a Laplacian of $[a_{ij}]_{n\times n}$. Let $\boldsymbol{p}_{\mathrm{c}} = \frac{1}{n}\sum_{i=1}^n \hat{\boldsymbol{p}}_{\mathrm{c},i}$ and $\boldsymbol{v}_{\mathrm{c}} = \frac{1}{n}\sum_{i=1}^n \hat{\boldsymbol{v}}_{\mathrm{c},i}$. Since $a_{ij} = a_{ji}$ for all $i, j \in \mathcal{V}$, $\dot{\boldsymbol{v}}_{\mathrm{c}} = \frac{1}{n}\sum_{i=1}^n \dot{\boldsymbol{v}}_{\mathrm{c},i} = -\boldsymbol{v}_{\mathrm{c}}$ holds. Denote $\hat{\boldsymbol{p}}_{\mathrm{c}} = \boldsymbol{\delta}_{\mathrm{p}} + \mathbf{1}_n \otimes \boldsymbol{p}_{\mathrm{c}}$ and $\hat{\boldsymbol{v}}_{\mathrm{c}} = \boldsymbol{\delta}_{\mathrm{v}} + \mathbf{1}_n \otimes \boldsymbol{v}_{\mathrm{c}}$, where $\boldsymbol{\delta}_{\mathrm{p}}$ and $\boldsymbol{\delta}_{\mathrm{v}} \in \mathbb{R}^{dn}$ are negotiation errors and satisfy $\boldsymbol{\delta}_{\mathrm{v}} = \dot{\boldsymbol{\delta}}_{\mathrm{p}}$. Substituting $\hat{\boldsymbol{p}}_{\mathrm{c}}$ and $\hat{\boldsymbol{v}}_{\mathrm{c}}$ into eq. (4) yields

$$\dot{\boldsymbol{\delta}}_{\mathrm{v}} = -c_1\tilde{\boldsymbol{L}}\boldsymbol{\delta}_{\mathrm{p}} - (c_2\tilde{\boldsymbol{L}} + \boldsymbol{I}_{dn})\boldsymbol{\delta}_{\mathrm{v}} - \mathbf{1}_n \otimes (\dot{\boldsymbol{v}}_{\mathrm{c}} + \boldsymbol{v}_{\mathrm{c}}). \tag{5}$$

Here, note that $\tilde{\boldsymbol{L}}(\mathbf{1}_n \otimes \boldsymbol{p}_{\mathrm{c}}) = 0$ and $\tilde{\boldsymbol{L}}(\mathbf{1}_n \otimes \boldsymbol{v}_{\mathrm{c}}) = 0$ due to $a_{ij} = a_{ji}$ for all $i, j \in \mathcal{V}$. Since $\dot{\boldsymbol{v}}_{\mathrm{c}} = \frac{1}{n}\sum_{i=1}^n \dot{\boldsymbol{v}}_{\mathrm{c},i} = -\boldsymbol{v}_{\mathrm{c}}$, the error dynamics (eq. (5)) can be expressed as follows:

$$\begin{bmatrix} \dot{\boldsymbol{\delta}}_{\mathrm{p}} \\ \dot{\boldsymbol{\delta}}_{\mathrm{v}} \end{bmatrix} = \begin{bmatrix} 0 & \boldsymbol{I}_{dn} \\ -c_1\tilde{\boldsymbol{L}} & -(c_2\tilde{\boldsymbol{L}} + \boldsymbol{I}_{dn}) \end{bmatrix} \begin{bmatrix} \boldsymbol{\delta}_{\mathrm{p}} \\ \boldsymbol{\delta}_{\mathrm{v}} \end{bmatrix}. \tag{6}$$

Let λ be an eigenvalue of eq. (6). The characteristic equation is given by $\det((\lambda^2 + \lambda)\boldsymbol{I}_{dn} + (\lambda c_2 + c_1)\tilde{\boldsymbol{L}}) = 0$. Then, the roots of the above equation can be obtained by solving $\lambda^2 + \lambda = (\lambda c_2 + c_1)\sigma$ where σ is an eigenvalue of $-\tilde{\boldsymbol{L}}$. Thus, we obtain:

$$\lambda = \frac{1}{2}\left[c_2\sigma - 1 \pm \sqrt{(c_2\sigma - 1)^2 + 4c_1\sigma}\right]. \tag{7}$$

Note that λ in eq. (7) has a similar form as eq. (15) in ref. [41]. As a result, it can follow a proof similar to Lemma 4.6 in ref. [41] to show that $\hat{\boldsymbol{p}}_{\mathrm{c},i}(\infty) = \boldsymbol{p}_{\mathrm{c}}$ and $\hat{\boldsymbol{v}}_{\mathrm{c},i}(\infty) = 0$ if $\sigma \geqslant 0$ and $\sum_{i=1}^n \hat{\boldsymbol{v}}_{\mathrm{c},i}(0) = 0$ by Assumption 2.

3.2 Tracking moving virtual group center

To track the virtual-maneuvering group center, we introduce a small number of informed robots who know the navigation information of a time-varying reference to be tracked. The basic idea is that the informed robots would insist on their interpretations of the desired motion during the negotiation process. As a result, the interpretations of the other uninformed ones would converge to those of the informed ones.

Let $\boldsymbol{p}_{\mathrm{t}}, \boldsymbol{v}_{\mathrm{t}} \in \mathbb{R}^d$ denote the position and velocity of a time-varying reference for the virtual group center. If robot i is informed, then it applies the following protocol to update its position interpretation:

$$\begin{aligned}\dot{\hat{\boldsymbol{v}}}_{\mathrm{c},i} = &-\sum_{j\in\mathcal{N}_i} a_{ij}\left[c_1\left(\hat{\boldsymbol{p}}_{\mathrm{c},i} - \hat{\boldsymbol{p}}_{\mathrm{c},j}\right) + c_2\left(\hat{\boldsymbol{v}}_{\mathrm{c},i} - \hat{\boldsymbol{v}}_{\mathrm{c},j}\right)\right] \\ &- \left[c_1\left(\hat{\boldsymbol{p}}_{\mathrm{c},i} - \boldsymbol{p}_{\mathrm{t}}\right) + c_2\left(\hat{\boldsymbol{v}}_{\mathrm{c},i} - \boldsymbol{v}_{\mathrm{t}}\right) - \dot{\boldsymbol{v}}_{\mathrm{t}}\right],\end{aligned} \tag{8a}$$

and uninformed robots execute a variant of protocol (eq. (3)) as follows:

$$\begin{aligned}\dot{\hat{\boldsymbol{v}}}_{\mathrm{c},i} = &-\sum_{j\in\mathcal{N}_i} a_{ij}\left[c_1\left(\hat{\boldsymbol{p}}_{\mathrm{c},i} - \hat{\boldsymbol{p}}_{\mathrm{c},j}\right) + c_2\left(\hat{\boldsymbol{v}}_{\mathrm{c},i} - \hat{\boldsymbol{v}}_{\mathrm{c},j}\right)\right] \\ &+ \frac{1}{\gamma_i}\sum_{j\in\mathcal{N}_i} a_{ij}\dot{\boldsymbol{v}}_{\mathrm{c},j},\end{aligned} \tag{8b}$$

where c_1 and c_2 are the same as those in eq. (3). The role of the first term in protocol (eq. (8)) is the same as that in eq. (3). The second term in eq. (8a) aims to track the time-varying reference and the second term in eq. (8b) is to align robots' own interpretations with neighboring ones. Next, we prove the convergence of eq. (8) by Theorem 2.

Theorem 2 Under Assumption 2, the position interpretations under negotiation protocol (eq. (8)) converge to the time-varying reference globally and asymptotically.

Proof. Denoting new states as $\hat{\boldsymbol{p}}_{\mathrm{c},n+1} \triangleq \boldsymbol{p}_{\mathrm{t}}$ and $\hat{\boldsymbol{v}}_{\mathrm{c},n+1} \triangleq \boldsymbol{v}_{\mathrm{t}}$, we rewrite negotiation protocol (eq. (8)) as

$$\dot{\hat{\boldsymbol{v}}}_{\mathrm{c},i} = -\sum_{j=1}^{n+1} a_{ij}\left[c_1\left(\hat{\boldsymbol{p}}_{\mathrm{c},i}-\hat{\boldsymbol{p}}_{\mathrm{c},j}\right)+c_2\left(\hat{\boldsymbol{v}}_{\mathrm{c},i}-\hat{\boldsymbol{v}}_{\mathrm{c},j}\right)-\frac{1}{\gamma_i}\dot{\boldsymbol{v}}_{\mathrm{c},j}\right], \quad (9)$$

where $a_{i,n+1} = 1$ for informed robot and $a_{i,n+1} = 0$ for uninformed one. In special, $a_{n+1,n+1} = 1$. Recall that $c_2 = \alpha_1 + c_1/(\alpha_1\gamma_i)$ in eq. (9). Reorganizing and multiplying γ_i on both sides of eq. (9) gives

$$\begin{aligned}&\sum_{j\in\mathcal{N}_i} a_{ij}\left[\frac{c_1}{\alpha_1}\left(\hat{\boldsymbol{v}}_{\mathrm{c},i}-\hat{\boldsymbol{v}}_{\mathrm{c},j}\right)+\left(\dot{\hat{\boldsymbol{v}}}_{\mathrm{c},i}-\dot{\hat{\boldsymbol{v}}}_{\mathrm{c},j}\right)\right]\\&=-\beta\sum_{j\in\mathcal{N}_i} a_{ij}\left[\frac{c_1}{\alpha_1}\left(\hat{\boldsymbol{p}}_{\mathrm{c},i}-\hat{\boldsymbol{p}}_{\mathrm{c},j}\right)+\left(\hat{\boldsymbol{v}}_{\mathrm{c},i}-\hat{\boldsymbol{v}}_{\mathrm{c},j}\right)\right],\end{aligned}$$

where $\beta = \alpha_1\gamma_i > 0$. Let

$$\boldsymbol{\varepsilon}_i = \sum\nolimits_{j\in\mathcal{N}_i} a_{ij}\left[\left(\hat{\boldsymbol{p}}_{\mathrm{c},i}-\hat{\boldsymbol{p}}_{\mathrm{c},j}\right)+\left(\hat{\boldsymbol{v}}_{\mathrm{c},i}-\hat{\boldsymbol{v}}_{\mathrm{c},j}\right)\right]$$

for i. Then, we have $\dot{\boldsymbol{\varepsilon}}_i = -\beta\boldsymbol{\varepsilon}_i$, which implies that $\boldsymbol{\varepsilon}_i$ is asymptotically and globally stable. Equivalently, it follows that $\hat{\boldsymbol{p}}_{\mathrm{c},i}$ and $\hat{\boldsymbol{v}}_{\mathrm{c},i}$ converge to $\boldsymbol{p}_{\mathrm{t}}$ and $\boldsymbol{v}_{\mathrm{t}}$ asymptotically and globally, respectively.

Some discussion about the negotiation algorithms is given below. First, the negotiation process can be viewed as a fast inner loop of the entire swarm system, and the control process as discussed later can be viewed as a slow outer loop of the entire system, as shown in Figure 1(a). As long as the inner loop enables robots to reach a consensus on the final virtual group center, the outer loop can control robots to form a cohesive swarm. Second, the control process uses the output of the negotiation process as the only input, and the negotiation process does not rely on the control process, as shown in Figure 1(a). In other words, the control process is only affected by the virtual group center. By this way, robots can gather around the virtual group center to form a coherent swarm, which will be presented in the next section.

4 Shepherding-inspired swarm control

Previously, we have defined the distributed negotiation mechanism of the virtual group center, and then we present shepherding-inspired swarm controller. The proposed control strategy is illustrated in Figure 1(c). To do that, we first require addressing the problem of how to determine whether a robot is a herding robot or a herded robot. Then, we need to solve the problem of how to design local interaction behaviors for muti-robot swarm control based on local information.

4.1 Robot role determination

Regarding the role of a robot, we here determine it according to the robot's location in the group. More specifically, we define the herding robots as ones who are at the boundary of the group, and the herded robots as ones who are located inside the group, as shown in Figure 2.

A question that immediately follows is how to distinguish whether a robot is at the boundary or inside the group. For this purpose, we identify it by using the number of line-of-sight neighbors. The definition of the line-of-sight neighbor of a robot will be given by eq. (11) later. Recall the metric neighbor set $\mathcal{N}_i$ defined by eq. (2). The metric neighbors of a robot are determined by the distance from it, as illustrated in Figure 2(a). Next, we identify the line-of-sight neighbors from these metric neighbors by partitioning the robot's vision area.

Let m denotes the number of divisions of the robot's vision area. See Figure 2(b) for an illustration. Then, the neighbor subset of the divided subarea k can be given as follows inspired by ref. [42]:

$$\mathcal{N}_i^k = \left\{j : \frac{2\pi}{m}(k-1) < \left\langle\theta_{ij}-\theta_i\right\rangle \leqslant \frac{2\pi}{m}k, j\in\mathcal{N}_i\right\},$$

where θ_i is the orientation of robot i, and θ_{ij} is the azimuth angle of neighbor j relative to robot i. The operator $\langle z\rangle$ transforms angle z into $[0, 2\pi)$. In each neighbor subset $\mathcal{N}_i^k$, we take the individual closest to robot i as the line-of-sight neighbor in vision subarea k (Figure 2(b)), that is

$$\widetilde{\mathcal{N}}_i^k = \left\{j' : j' = \arg\min\left\|\boldsymbol{p}_i-\boldsymbol{p}_j\right\|, j\in\mathcal{N}_i^k\right\}. \quad (10)$$

Recall that $\|\cdot\|$ refers to the Euclidean norm in $\mathbb{R}^d$. As a result, the line-of-sight neighbor set of robot i is defined by

$$\widetilde{\mathcal{N}}_i = \left\{j : j\in\widetilde{\mathcal{N}}_i^k, k = 1, 2, ..., m\right\}. \quad (11)$$

It follows from eq. (11) that $\widetilde{\mathcal{N}}_i \subset \mathcal{N}_i$. Here, we take $m = 6$ as shown in Figure 2(b), which is inspired by the visibility interactions in the natural swarm. The work in ref. [43] shows that starlings only interact with 6 or 7 nearby starlings rather than all individuals within the vision, which is related to individual tracking ability and survivability.

As can be seen from eq. (11), it has at most m line-of-sight neighbors for robot i, namely $|\widetilde{\mathcal{N}}_i| \leqslant m$. By this way, we can determine the role of a robot according to the number of its surrounding line-of-sight neighbors. To this end, we make the following definition.

(1) Herding robot. A robot with less than m line-of-sight neighbors is called a Herding robot, which means that it is at the boundary of the group. As shown in Figure 2(c), the focus robot is a herding robot since there are 5 ($m = 6$) line-of-sight neighbors around it.

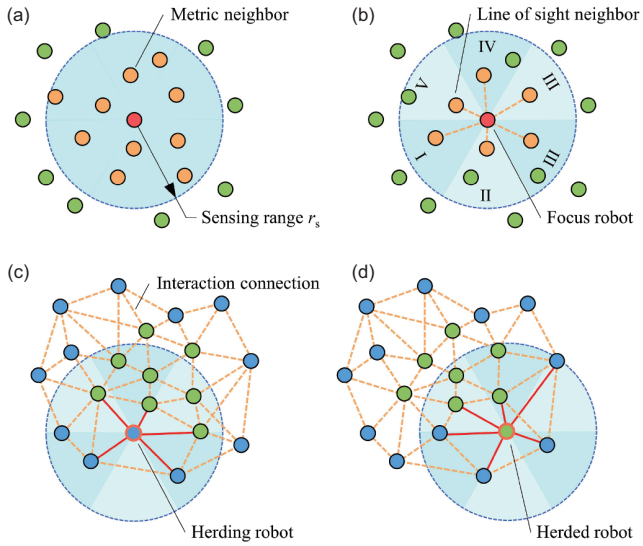

Figure 2 Schematic diagram of robot role determination. (a) Metric-based neighboring robots. The focus robot is red. Orange robots are the metric neighbors of the focus robot. (b) Line-of-sight neighboring robots. The vision area of the focus robot is divided into six subareas. Orange robots are line-of-sight neighbors of the focus robot. (c), (d) Examples to explain the herding robot and herded robot. Herding robots are blue and herded robots are green.

(2) Herded robot. A robot with m line-of-sight neighbors is called Herded robot, which implies that it is located inside the robot group. As shown in Figure 2(d), there are 6 line-of-sight neighbors around the focus robot, and thus it is called a herded robot.

Next, we discuss the connectivity of subgraph $\widetilde{\mathcal{G}} = (\mathcal{V}, \widetilde{\mathcal{E}})$ defined by $\widetilde{\mathcal{E}} = \{(i, j) : i \in \mathcal{V}, j \in \widetilde{\mathcal{N}}_i\}$ through Theorem 3. This result is used later in Section 4.2 to prove the convergence of the control law.

Lemma 2 If robot l is a line-of-sight neighbor of robot i in vision subarea k, then any other metric neighbors j of robot i in subarea k are closer to the robot j than robot i.

Proof. Denote $d_{ij} = \|\boldsymbol{p}_i - \boldsymbol{p}_j\|$ as the distance between robot i and j. By applying the Cosines law, we have $d_{lj}^2 = d_{il}^2 + d_{ij}^2 - 2d_{il}d_{ij}\cos\phi$ where ϕ is the angle between vectors $\boldsymbol{p}_l - \boldsymbol{p}_i$ and $\boldsymbol{p}_j - \boldsymbol{p}_i$. Recall that m is taken to be 6, which means $\phi \leqslant \pi/3$. Then, we have

$$d_{lj}^2 \leqslant d_{il}^2 + d_{ij}^2 - d_{il}d_{ij} = d_{ij}^2 - d_{il}\left(d_{ij} - d_{il}\right).$$

It follows from eq. (10) that $d_{il} \leqslant d_{ij}$. Thus, we can conclude that $d_{lj}^2 \leqslant d_{ij}^2$, that is $d_{lj} \leqslant d_{ij}$, completing the proof.

Theorem 3 Consider a subgraph $\widetilde{\mathcal{G}} = (\mathcal{V}, \widetilde{\mathcal{E}})$ of graph $\mathcal{G} = (\mathcal{V}, \mathcal{E})$, where $\widetilde{\mathcal{E}} = \{(i, j) : i \in \mathcal{V}, j \in \widetilde{\mathcal{N}}_i\}$. If $\mathcal{G}$ is connected for all $t \geqslant 0$, then $\widetilde{\mathcal{G}}$ remains connected for all time.

Proof. The idea of the proof is to show that for any pair $(i, j) \in \mathcal{E}$ in $\mathcal{G}$, there always exists a path from j to i in $\widetilde{\mathcal{G}}$. Here, assume j is any metric neighbor of robot i. This means that robot i can keep connected with j via a multi-hop path constituted by a set of line-of-sight neighbors. Then, we prove that there exists a path from j to i in $\widetilde{\mathcal{G}}$.

Suppose that robot j is in subarea k of robot i and robot l is the line-of-sight neighbor of robot i in this subarea. Since $\|\boldsymbol{p}_l - \boldsymbol{p}_j\| \leqslant \|\boldsymbol{p}_i - \boldsymbol{p}_j\|$ by applying Lemma 2, robot j is also a neighbor in a certain subarea of robot l. At this time, if robot j is a line-of-sight neighbor of robot l, then the theorem holds. Otherwise, we continue to find a line-of-sight neighbor for robot l's line-of-sight neighbor denoted as robot s. As this process is repeated, the distance between robots s and j decreases based on Lemma 2. As a result, we can always find a line-of-sight robot such that robot j is the nearest neighbor in one of its vision subarea. In other words, we can find a path consisting of line-of-sight neighbors between robot i and j, completing the proof.

4.2 Swarm control law design

Inspired by the natural shepherding behaviors, we design the following control strategy for distributed swarm control of massive robots:

$$\boldsymbol{u}_i = \boldsymbol{f}_i^{\text{inter}} + \boldsymbol{f}_i^{\text{herd}} + \boldsymbol{f}_i^{\text{align}}, \tag{12}$$

where $\boldsymbol{f}_i^{\text{inter}}$, $\boldsymbol{f}_i^{\text{herd}}$, and $\boldsymbol{f}_i^{\text{align}}$ represent attraction-repulsion force, swarm-herding force, and velocity-alignment force, respectively.

(1) Attraction-repulsion force. The first component is the attraction-repulsion force $\boldsymbol{f}_i^{\text{inter}}$, which describes the internal attraction and repulsion interactions among robots, as shown in Figure 1(c). In particular, it is designed as

$$\boldsymbol{f}_i^{\text{inter}} = \sum_{j \in \widetilde{\mathcal{N}}_i} \left[\kappa_1 \frac{\rho(\|\boldsymbol{p}_i - \boldsymbol{p}_j\|)}{\|\boldsymbol{p}_i - \boldsymbol{p}_j\|_\epsilon} - \kappa_2 \frac{\rho(\|\boldsymbol{p}_i - \boldsymbol{p}_j\|)^2}{\|\boldsymbol{p}_i - \boldsymbol{p}_j\|_\epsilon^2} \right] \boldsymbol{n}_{ij}, \tag{13}$$

with

$$\rho(z) = \frac{3}{\sqrt{2\pi}(r_s - r_b)} \exp\left(-\frac{9}{2} \left(\frac{z - r_b}{r_s - r_b} \right)^2 \right),$$

where κ_1 and κ_2 are two positive constants, and $\boldsymbol{n}_{ij} = (\boldsymbol{p}_j - \boldsymbol{p}_i)/\|\boldsymbol{p}_j - \boldsymbol{p}_i\|$ is a unit vector. The operator $\|z\|_\epsilon$ is defined by $\|z\|_\epsilon = \sqrt{z^{\mathrm{T}} z + \epsilon}$ with a small number $\epsilon > 0$. The use of $\widetilde{\mathcal{N}}_i$ is to allow robots to pay attention to the neighbors who have great impacts on themselves, and meanwhile it also conforms to the practical characteristics of onboard sensors with local measurement capability.

The force $\boldsymbol{f}_i^{\text{inter}}$ acts as both attraction and repulsion forces within the multi-robot system, which can drive robots to form a tight group, as shown in Figure 1(c). If one robot is close to another robot, mutual attraction occurs between these two robots to drive them closer, as seen from the first term in

brackets of eq. (13). We refer to this behavior as attraction interaction. If approached by another robot infinitely, the focal robot pushes it away from another one to avoid a collision, as seen from the second term in brackets of eq. (13). We refer to this behavior as repulsion interaction. For a better understanding, an illustrative example is introduced to describe the attraction and repulsion interactions among nearby robots, as shown in Figure 1(c).

(2) Swarm-herding force. The most important component in control law (eq. (12)) is the swarm-herding force $\boldsymbol{f}_i^{\text{herd}}$, the responsibility of which is to enclose the herded robots to assemble a cohesive swarm, as shown in Figure 1(c). In particular, it is defined as the following form:

$$\boldsymbol{f}_i^{\text{herd}} = \kappa_3 \varsigma_i \left(\hat{\boldsymbol{p}}_{\text{c},i} - \boldsymbol{p}_i\right) + \kappa_4 \left(\hat{\boldsymbol{v}}_{\text{c},i} - \boldsymbol{v}_i\right) + \dot{\hat{\boldsymbol{v}}}_{\text{c},i}, \tag{14}$$

where $\kappa_3, \kappa_4 > 0$ are two constants, and $\varsigma_i \in \{0, 1\}$ is used to mark whether robot i is a herding robot or a herded robot. If there is always a line-of-sight neighbor in each vision subarea around robot i, i.e., $|\widetilde{\mathcal{N}}_i| = m$, then robot i is denoted as a herded robot. At this time, ς_i is taken to be 0. If there exists at least one subarea without neighbors around robot i, $|\widetilde{\mathcal{N}}_i| < m$, then robot i is a herding robot and ς_i is taken to be 1. Recall that m is the number of divisions of robot i's vision area.

As seen from eq. (14), there are two objectives of the swarm-herding force $\boldsymbol{f}_i^{\text{herd}}$. On the one hand, if robot i is a herded robot ($\varsigma_i = 0$), it aims to maneuver at the same velocity with the virtual group center. At this time, only the second and third terms in eq. (14) come into play. On the other hand, if robot i is a herding robot ($\varsigma_i = 1$), then its purpose is to enclose the internal herded robots towards the virtual group center while maintaining the same velocity as the virtual group center. At this time, all the terms in eq. (14) are effective. An easy-to-understand example of $\boldsymbol{f}_i^{\text{herd}}$ can be found in Figure 1(c).

(3) Velocity-alignment force. The aim of velocity-alignment force $\boldsymbol{f}_i^{\text{align}}$ is to achieve velocity alignment with neighbors, as illustrated in Figure 1(c). To this end, it is designed as

$$\boldsymbol{f}_i^{\text{align}} = -\sum_{j \in \widetilde{\mathcal{N}}_i} \tilde{a}_{ij}\left(\boldsymbol{v}_i - \boldsymbol{v}_j\right), \tag{15}$$

where the adjacent weight $\tilde{a}_{ij}$ simulates the interaction strength between two adjacent robots, which is defined by

$$\tilde{a}_{ij} = \begin{cases} 1, & 0 \leqslant r_{ij} \leqslant 2r_{\text{b}}, \\ \dfrac{1}{2}\left[1 - \cos\left(\pi \dfrac{r_{ij} - 2r_{\text{b}}}{r_{\text{s}} - 2r_{\text{b}}}\right)\right], & 2r_{\text{b}} < r_{ij} < r_{\text{s}}, \\ 0, & r_{ij} \geqslant r_{\text{s}}, \end{cases} \tag{16}$$

where $r_{ij} = \|\boldsymbol{p}_i - \boldsymbol{p}_j\|$. It follows from eq. (16) that if robots i and j are close to each other, the interaction strength a_{ij} will increase. On the contrary, if r_{ij} increases, a_{ij} will decrease. If $r_{ij} \to r_{\text{s}}$, there is $a_{ij} \to 0$. The weight a_{ij} is introduced to facilitate separation between robots, that is, with weights decreasing to zero as robots separate [19], which is meaningful for swarm control.

As can be seen from eq. (15), $\boldsymbol{f}_i^{\text{align}}$ serves as a friction. Since the evolution direction of $\boldsymbol{f}_i^{\text{align}}$ is opposite to the direction of the relative velocity $\boldsymbol{v}_i - \boldsymbol{v}_j$, it will reduce the difference of the relative velocity until $\boldsymbol{v}_i$ and $\boldsymbol{v}_j$ reach a consistent velocity.

4.3 Convergence analysis

Up to now, we have achieved the design of the shepherding-inspired swarm controller. Then, we present the convergence analysis of the proposed control law as follows. Denote $\boldsymbol{p} = [\boldsymbol{p}_1^{\text{T}}, ..., \boldsymbol{p}_n^{\text{T}}]^{\text{T}}, \boldsymbol{v} = [\boldsymbol{v}_1^{\text{T}}, ..., \boldsymbol{v}_n^{\text{T}}]^{\text{T}} \in \mathbb{R}^{dn}$ and $\hat{\boldsymbol{p}}_{\text{c}} = [\hat{\boldsymbol{p}}_{\text{c},1}^{\text{T}}, ..., \hat{\boldsymbol{p}}_{\text{c},n}^{\text{T}}]^{\text{T}}, \hat{\boldsymbol{v}}_{\text{c}} = [\hat{\boldsymbol{v}}_{\text{c},1}^{\text{T}}, ..., \hat{\boldsymbol{v}}_{\text{c},n}^{\text{T}}]^{\text{T}} \in \mathbb{R}^{dn}$. The matrix-vector form of eq. (12) is

$$\dot{\boldsymbol{v}} = -\nabla V(\boldsymbol{p}) - \tilde{\boldsymbol{L}}\boldsymbol{v} + \kappa_3 \boldsymbol{\Omega}\left(\hat{\boldsymbol{p}}_{\text{c}} - \boldsymbol{p}\right) + \kappa_4\left(\hat{\boldsymbol{v}}_{\text{c}} - \boldsymbol{v}\right) + \dot{\hat{\boldsymbol{v}}}_{\text{c}}, \tag{17}$$

where ∇ is the gradient operator along $\boldsymbol{p}$, and matrix $\tilde{\boldsymbol{L}}$ and $\boldsymbol{\Omega}$ are defined by $\tilde{\boldsymbol{L}} = L \otimes \boldsymbol{I}_d$ and $\boldsymbol{\Omega} = \text{diag}(\varsigma_1, ..., \varsigma_n)$, respectively. Here, L is the Laplacian of $[\tilde{a}_{ij}]_{n\times n}$, and $\boldsymbol{I}_d$ is a d-dimensional identity matrix. The potential energy $V(\boldsymbol{p})$ of swarm system (eq. (1)) is defined by

$$V(\boldsymbol{p}) = \sum_{i=1}^{n} \sum_{j \in \widetilde{\mathcal{N}}_i} \int_{\Gamma_i} \left[\kappa_2 \frac{\rho(\|\boldsymbol{p}_i - \boldsymbol{p}_j\|)^2}{\|\boldsymbol{p}_i - \boldsymbol{p}_j\|_\epsilon^2} - \kappa_1 \frac{\rho(\|\boldsymbol{p}_i - \boldsymbol{p}_j\|)}{\|\boldsymbol{p}_i - \boldsymbol{p}_j\|_\epsilon}\right] \boldsymbol{n}_{ij} \text{d}\boldsymbol{p}_i,$$

where Γ_i is the motion trajectory of robot i. The boundedness of functions is discussed as below.

Lemma 3 The function $V(\boldsymbol{p})$ is bounded for all $\boldsymbol{p} \in \mathbb{R}^{dn}$.

Proof. The design of $V(\boldsymbol{p})$ has a similar form as that in eq. (3) in ref. [11]. By applying the Lemma 5 in ref. [11], one can conclude that there exists $h, c \in \mathbb{R}$ such that $h \leqslant V(\boldsymbol{p}) \leqslant c$ holds for all $\boldsymbol{p} \in \mathbb{R}^{dn}$.

With the above presentation, we are ready to present the convergence of control law (eq. (17)). To do that, we need to introduce an assumption of $\mathcal{G}$ as shown in Assumption 2. The assumption is essential when the initial graph $\mathcal{G}$ is fixed and connected and the negotiation process of the virtual group center converges much faster than the swarm control process. By this way, we suppose that the negotiation process has already converged when analyzing the control process, thus making Assumption 1. Then, we analyze the convergence of eq. (17) by Theorem 4.

Theorem 4 Under Assumptions 1 and 2, the swarm robots can form an equilibrium configuration, i.e., (1) there

exists $r > 0$ such that $\|\boldsymbol{p}_i - \hat{\boldsymbol{p}}_c\| \leqslant r$ for all $t \geqslant t_0$, and (2) as $t \to \infty$, it holds that $\|\boldsymbol{v}_i - \hat{\boldsymbol{v}}_c\| = 0$ for any $i \in \mathcal{V}$.

Proof. Let $\boldsymbol{\chi} = \hat{\boldsymbol{p}}_c - \boldsymbol{p}$ and $\boldsymbol{\upsilon} = \hat{\boldsymbol{v}}_c - \boldsymbol{v}$. Then, the matrix-vector form of system (eq. (1)) applying (eq. (17)) is formulated as

$$\begin{cases} \dot{\boldsymbol{\chi}} = \boldsymbol{\upsilon}, \\ \dot{\boldsymbol{\upsilon}} = -\nabla U(\boldsymbol{\chi}) - \tilde{\boldsymbol{L}}\boldsymbol{\upsilon} + \kappa_4 \boldsymbol{\upsilon}, \end{cases} \tag{18}$$

where $U(\boldsymbol{\chi}) = V(\boldsymbol{\chi}) + \frac{1}{2}\kappa_3 \boldsymbol{\Omega}\boldsymbol{\chi}^{\mathrm{T}}\boldsymbol{\chi}$. Here, $\tilde{\boldsymbol{L}}$ is positive semidefinite according to Lemma 2. Then, we define a Lyapunov candidate of eq. (18) as

$$H(\boldsymbol{\chi}, \boldsymbol{\upsilon}) = U(\boldsymbol{\chi}) + \frac{1}{2}\boldsymbol{\upsilon}^{\mathrm{T}}\boldsymbol{\upsilon}. \tag{19}$$

By using Lemma 3 and Assumption 1, the initial Lyapunov $H(\boldsymbol{\chi}(t_0), \boldsymbol{\upsilon}(t_0))$ is finite, denoted as H_1. Eqs. (18) and (19) have a similar form as eqs. (20) and (21) in our previous work [11]. As a result, it can follow a proof similar to Theorem 3 in ref. [11] to show that $\|\boldsymbol{p}_i - \hat{\boldsymbol{p}}_c\| \leqslant \sqrt{2(H_1 - h)/\kappa_3}$ for all $t \geqslant t_0$ and $\|\boldsymbol{v}_i(\infty) - \hat{\boldsymbol{v}}_c(\infty)\| = 0$ hold for any $i \in \mathcal{V}$, completing the proof.

5 Numerical and flight simulations

To verify the theoretical results, we implement and text our proposed swarm scheme in both numerical and flight simulations. The details are given as below.

5.1 Performance metrics

To evaluate the performance of our proposed scheme, we define the following performance metrics.

The first metric, uniformity, is to evaluate the distribution uniformity of robots. Let $j = \arg\min_{k \in \mathcal{N}_i} \|\boldsymbol{p}_i - \boldsymbol{p}_k\|$ be the nearest neighbor to robot i. Then, the metric is defined as

$$M_1 = \sum_{i=1}^{n} \left(r_{ij} - \frac{1}{n} \sum\nolimits_{i=1}^{n} r_{ij} \right),$$

where $r_{ij} = \left\|\boldsymbol{p}_i - \boldsymbol{p}_j\right\|$. The metric M_1 reaches zero when the distance of any two adjacent robots tend to be the same.

The second metric, swarm radius, is the minimum radius of a sphere centered at group center that contains all the robots. In particular, the metric is defined as

$$M_2 = \max_{i \in \mathcal{V}} \left\| \boldsymbol{p}_i - \sum\nolimits_{j=1}^{n} \boldsymbol{p}_j \right\|.$$

If robots form an aggregated swarm, M_2 eventually converges to a fixed value. Otherwise, M_2 diverges.

The third metric, velocity polarization, is to evaluate the polarization of the velocities of the robot swarm. The metric is defined as

$$M_3 = \frac{\| \sum_{i=1}^{n} \boldsymbol{v}_i \|}{\sum_{i=1}^{n} \|\boldsymbol{v}_i\|}.$$

If all the robots move coherently in same velocity, then M_3 is close to one. On the contrary, if all the robots move chaotically, then M_3 is approximately zero.

5.2 Numerical simulation

We present two simulation examples as below to test and verify the effectiveness and maneuverability of our proposed scheme. In simulation, each robot is modeled as a circular omnidirectional robot with a body size $r_b = 1.5$ m. Robots can sense any other robot who lies within its sensing range $r_s = 8.4$ m.

The first example is used to evaluate the effectiveness of our proposed scheme for swarm control of massive robots. In this example, we compare the proposed scheme with two state-of-the-art methods. The first is the well-known Olfati scheme [22] and the second is our previous scheme [11]. The parameter settings of these three methods are listed in Table 1. As illustrated in Figure 3, we set up 4 different cases for comparisons, corresponding to 4 different initial configurations and 3 types of swarm size. It is shown that, given the same initial configurations, three schemes can assemble an aggregated swarm when the number of robots is as small as 10. At this time, the uniformity between robots is consistent, while the swarm formed by our method are more compact, as demonstrated in Figure 3(b). However, as the swarm size increases, fragmentation will occur in Olfati scheme, which is consistent with the conclusion in ref. [22]. In contrast, the method in ref. [11] is suitable for swarm control of a large number of robots. However, the fragmentation phenomenon also occurs when the initial positions of robot swarm are sparse, as shown in Case 2 of Figure 3(a). Furthermore, the method in ref. [11] also causes void phenomenon, as shown in Case 4 of Figure. 3(a). Different from the above two

Table 1 Simulation parameters

Method in ref. [22]		Method in ref. [11]		Our proposed	
d	7.0	r_s	1.5	r_b	1.5
r	8.4	r_c	8.4	r_s	8.4
a	5	α	51	κ_1	51
b	5	β	151	κ_2	151
c	4.5	–	–	c_1	4
h	0.2	–	–	α_1	6
–	–	–	–	κ_3	0.45
–	–	–	–	κ_4	2.36

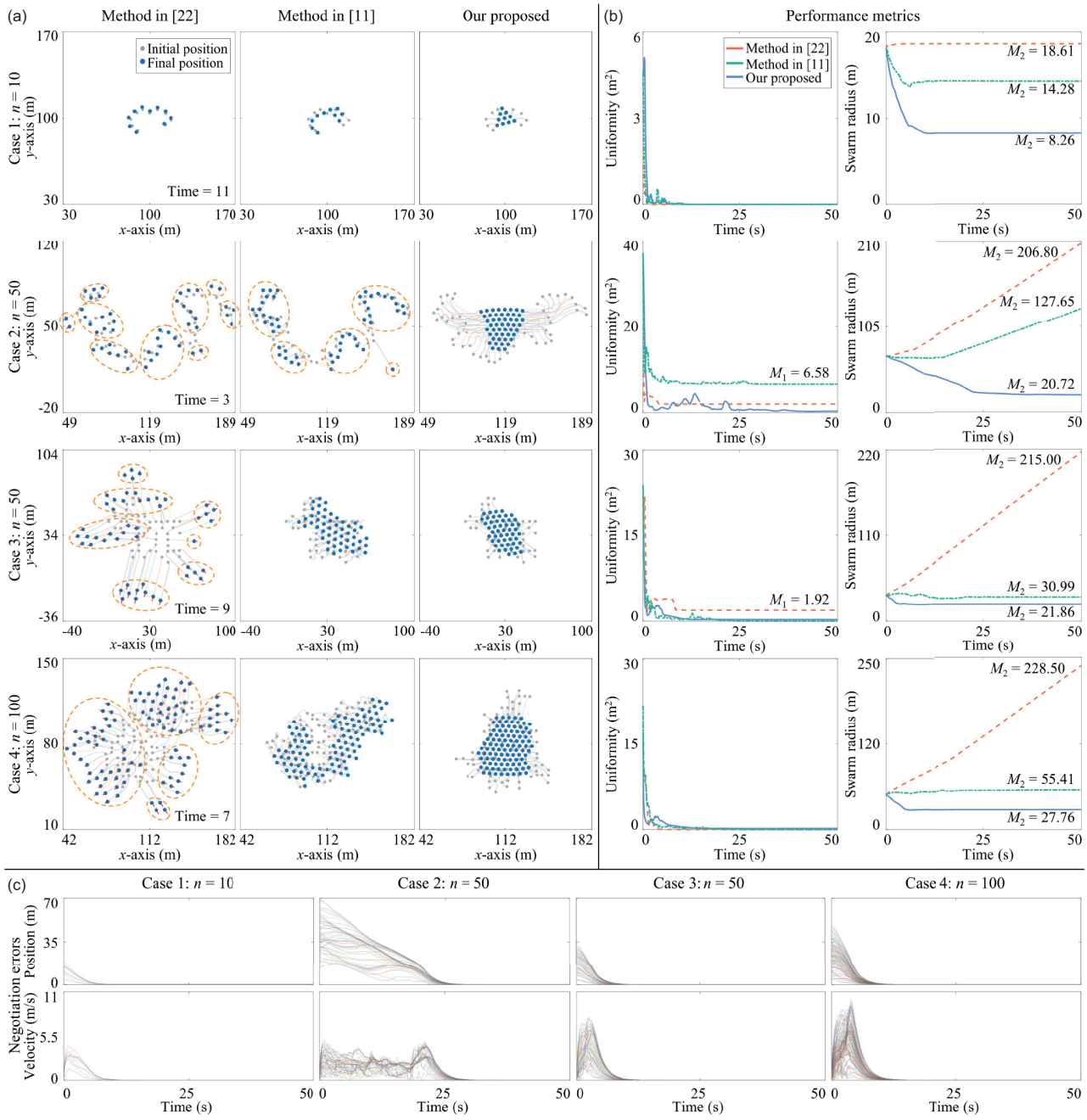

Figure 3 Comparison between our proposed method, Olfati method [22], and our previous method [11]. (a) Final configurations and trajectories of the swarm control by the three methods. (b) Performance metrics of comparison results. (c) Negotiation errors of the position and velocity with the means of all the robots' initial interpretations of our proposed method.

methods, our proposed scheme can form an integrity, uniformity, and stability configuration without fragmentation and void phenomena. Moreover, the final configuration is relatively tighter, as demonstrated in Figure 3(b). It is also shown that the position interpretations on the virtual group center of all the robots converge to the means of their initial interpretations and the velocity interpretations converge to zero, as shown in Figure 3(c).

The second simulation example demonstrates the motion property of our method in terms of translation and rotation. As shown in Figure 4, we set up a scenario where robot swarm tracks a moving virtual group center. In this example, only one fifth of the robots are informed robots who know the navigation information of a time-varying reference to be tracked, and other robots, uninformed robots, do not require knowing who the informed robots are. As can be seen, robots swarm can form an aggregated and orderly swarm from an initially disordered configuration and track a time-varying reference stably. Moreover, the equilibrium configuration of robot swarm is formed by the way that herding robots enclose

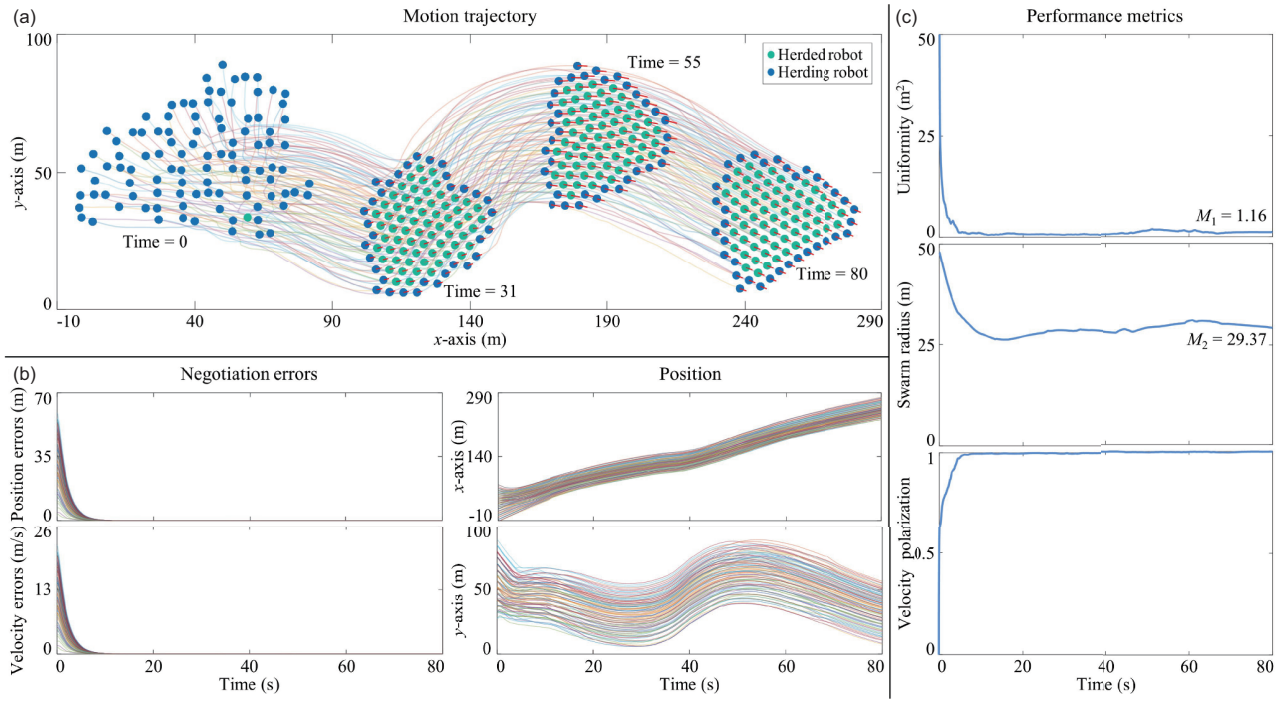

Figure 4 Simulation results to illustrate the maneuverability of the proposed swarm scheme. (a) Swarm trajectories for tracking moving virtual group center. (b) Negotiation errors and motion states of the maneuvering swarming. (c) Performance metrics of the maneuvering process.

internal herded robots. As shown in Figure 4(a), the green circle represents the herded robot and the blue one is the herding robot, which is dynamically determined by the number of its line-of-sight neighbors. It can also be found that all the robots are evenly distributed by this way. Most importantly, each robot's interpretation on the virtual group center can quickly tend to be consistent and converge to the time-varying reference, which is an important basis for achieving swarm aggregation. Moreover, the negotiation results of each robot do not fluctuate with the movement of robot swarm.

5.3 Flight simulation

To validate the efficiency of our proposed scheme, we perform a high-fidelity simulation using the AirSim simulator built on Unreal Engine that offers physical simulations. AirSim is an open-source platform that aims to bridge the gap between simulation and reality [44].

In order to adapt to aerial robots, we design the following conversion to convert acceleration commands into pitch angle θ_i, roll angle ϕ_i and throttle τ_i of aerial robot i:

$$\begin{cases} \theta_i = \arcsin \dfrac{-u_{x,i}}{T}, \\ \phi_i = \arcsin \dfrac{u_{y,i}}{T\cos\theta_i}, \\ \tau_i = \kappa_5(p_{z,i} - p^{\mathrm{r}}_{z,i}) + \kappa_6 v_{z,i} + \tau^{\mathrm{r}}_i, \end{cases}$$

where $u_{x,i}$ and $u_{y,i}$ represent the components of $\boldsymbol{u}_i$ along x-axis and y-axis respectively, and $p_{z,i}$ and $v_{z,i}$ are the components of position $\boldsymbol{p}_i$ and velocity $\boldsymbol{v}_i$ along z-axis, and $\kappa_5, \kappa_6 > 0$ are positive constants. Moreover, T indicates the main thrust given by the four rotors. In this simulation, we mainly consider horizontal flight at a specified altitude $p^{\mathrm{r}}_{z,i}$, thus T can be obtained by $T = mg/(\cos\theta\cos\phi)$. Here, m is the mass of an aerial robot and g is the acceleration due to gravity. The constant τ^{r}_i represents the throttle reference when a quadcopter is hovering at $p^{\mathrm{r}}_{z,i}$. It should be noted that axes x, y, and z correspond to north, east, and ground respectively

Figure 5 shows the example to verify the proposed scheme for aerial robot swarm. At the beginning, robots are randomly distributed, and the graph formed by their positions is initially connected. Then, all the robots take off in batches and climb to the specified altitude −20 m. Next, each robot gradually forms a gathered swarm through local interactions and moves to the target reference at a speed of 2 m/s. In this simulation, we demonstrate that our proposed scheme can be easily extended to aerial robots, and it can provide reliable performance.

6 Conclusion

In this article, we proposed an integrated negotiation-control scheme for distributed swarm control inspired by the shepherding behaviors. The proposed swarm scheme can prevent

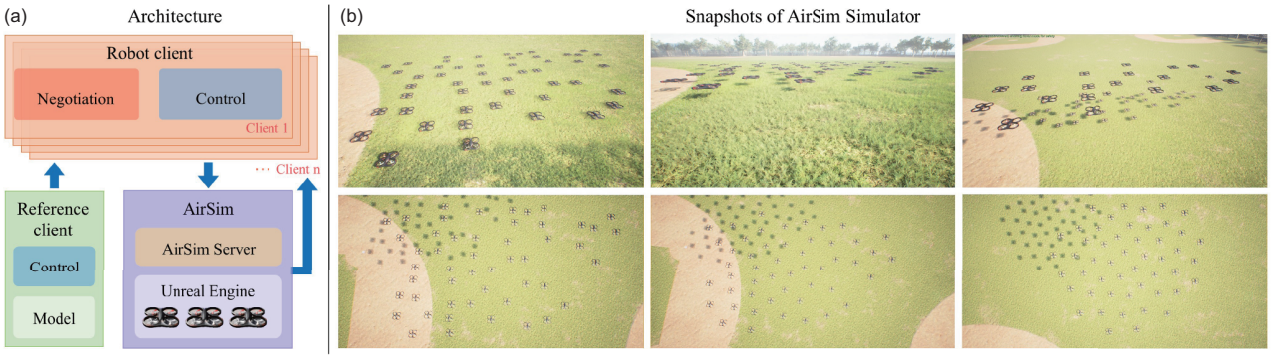

Figure 5 Flight simulation of the proposed scheme. (a) Architecture of the simulation. (b) Snapshots of 50 aerial robots forming an equilibrium swarm.

robot swarms from trapping in a local minimum caused by local observations, such as fragmentation and void phenomena. To be specific, herding robots enclose the internal herded robots by gathering towards their virtual group center, and then forming a collective swarm. The introduction of the virtual group center obtained by local negotiations with neighbors, enables robots to have a broader global observation capability. In this case, robots can make comprehensive tradeoffs from a global perspective in motion decision-making. In addition, we also present both numerical and flight simulations to demonstrate the correctness and effectiveness of our proposed control laws. The results show that our scheme provides effective improvement of integrity, uniformity, and stability for swarm control. In future work, we will incorporate the predefined time consensus into the negotiation process, and consider time delays and disturbances in practical networked systems.

This work was supported by the National Key R&D Program of China (Grant No. 2022YFB3305600), the National Natural Science Foundation of China (Grant Nos. 62103015 and 62141604), the China Postdoctoral Science Foundation (Grant No. 2023M740185), and the Postdoctoral Fellows of Beihang "Zhuoyue" Program.

1 Vicsek T, Zafeiris A. Collective motion. Phys Rep, 2012, 517: 71–140
2 Chen Y, Kolokolnikov T. A minimal model of predator-swarm interactions. J R Soc Interface, 2014, 11: 20131208
3 Chuang Y L, Huang Y R, D'Orsogna M R, et al. Multi-vehicle flocking: Scalability of cooperative control algorithms using pairwise potentials. In: Proceedings of the 2007 IEEE International Conference on Robotics and Automation. Rome: IEEE, 2007. 2291–2299
4 Yang J C, Lu Q S, Lang X F. Flocking shape analysis of multi-agent systems. Sci China Tech Sci, 2010, 53: 741–747
5 Tang Y, Hu Y, Cui J, et al. Vision-aided multi-UAV autonomous flocking in GPS-denied environment. IEEE Trans Ind Electron, 2019, 66: 616–626
6 Xu Y, Luo D L, You Y C, et al. New advances in multiple autonomous aerial robots formation control technology. Sci China Tech Sci, 2019, 62: 1871–1872
7 Wang X, Lu J. Collective behaviors through social interactions in bird flocks. IEEE Circuits Syst Mag, 2019, 19: 6–22
8 Wang X X, Liu Z X, Chen Z Q. Event-triggered fault-tolerant consensus control with control allocation in leader-following multi-agent systems. Sci China Tech Sci, 2021, 64: 879–889
9 Yu Y P, Liu J C, Wei C. Hawk and pigeons intelligence for UAV swarm dynamic combat game via competitive learning pigeon-inspired optimization. Sci China Tech Sci, 2022, 65: 1072–1086
10 Li J, Li L, Zhao S. Predator-prey survival pressure is sufficient to evolve swarming behaviors. New J Phys, 2023, 25: 092001
11 Sun G, Zhou R, Di B, et al. A physicochemically inspired approach to flocking control of multiagent system. Nonlinear Dyn, 2020, 102: 2627–2648
12 Reynolds C W. Flocks, herds and schools: A distributed behavioral model. SIGGRAPH Comput Graph, 1987, 21: 25–34
13 Vicsek T, Czirók A, Ben-Jacob E, et al. Novel type of phase transition in a system of self-driven particles. Phys Rev Lett, 1995, 75: 1226–1229
14 Vásárhelyi G, Virágh C, Somorjai G, et al. Optimized flocking of autonomous drones in confined environments. Sci Robot, 2018, 3: eaat3536
15 Gómez-Nava L, Bon R, Peruani F. Intermittent collective motion in sheep results from alternating the role of leader and follower. Nat Phys, 2022, 18: 1494–1501
16 Romanczuk P, Couzin I D, Schimansky-Geier L. Collective motion due to individual escape and pursuit response. Phys Rev Lett, 2009, 102: 010602
17 Luo Q, Duan H. Distributed UAV flocking control based on homing pigeon hierarchical strategies. Aerosp Sci Tech, 2017, 70: 257–264
18 Cai H, Zhang T Y, Gao H L, et al. Cooperative driven algorithm for Couzin model based fish school by multiple predators. Wireless Commun Mobile Comput, 2022, 2022: 1494–1501
19 Cucker F, Smale S. Emergent behavior in flocks. IEEE Trans Autom Control, 2007, 52: 852–862
20 Yin X, Yue D, Chen Z. Asymptotic behavior and collision avoidance in the Cucker-Smale model. IEEE Trans Autom Control, 2020, 65: 3112–3119
21 Zhang Z, Yin X, Gao Z. Non-flocking and flocking for the Cucker-Smale model with distributed time delays. J Franklin Inst, 2023, 360: 8788–8805
22 Olfati-Saber R. Flocking for multi-agent dynamic systems: Algorithms and theory. IEEE Trans Autom Control, 2006, 51: 401–420
23 Saif O, Fantoni I, Zavala-Río A. Distributed integral control of multiple UAVs: Precise flocking and navigation. IET Control Theory Appl, 2019, 13: 2008–2017
24 Levine H, Rappel W J, Cohen I. Self-organization in systems of self-propelled particles. Phys Rev E, 2000, 63: 017101
25 Katz Y, Tunstrøm K, Ioannou C C, et al. Inferring the structure and dynamics of interactions in schooling fish. Proc Natl Acad Sci USA, 2011, 108: 18720–18725
26 Ling H, Mclvor G E, van der Vaart K, et al. Costs and benefits of social relationships in the collective motion of bird flocks. Nat Ecol Evol,

2019, 3: 943–948
27 Koren Y, Borenstein J. Potential field methods and their inherent limitations for mobile robot navigation. In: Proceedings of the 1991 IEEE International Conference on Robotics and Automation. Sacramento: IEEE, 1991. 1398–1404
28 Wang Z Y, Gu D B, Hu H S. Leader-follower flocking experiments using estimated flocking center. In: Proceedings of the 2009 International Conference on Mechatronics and Automation. Changchun: IEEE, 2009. 3733–3738
29 Gu D, Wang Z. Leader-follower flocking: Algorithms and experiments. IEEE Trans Control Syst Tech, 2009, 17: 1211–1219
30 Bhowmick C, Behera L, Shukla A, et al. Flocking control of multiagent system with leader-follower architecture using consensus based estimated flocking center. In: Proceedings of the IECON 2016 - 42nd Annual Conference of the IEEE Industrial Electronics Society. Florence: IEEE, 2016. 166–171
31 Zhao S, Dimarogonas D V, Sun Z, et al. A general approach to coordination control of mobile agents with motion constraints. IEEE Trans Autom Control, 2018, 63: 1509–1516
32 Sun G, Zhou R, Ma Z, et al. Mean-shift exploration in shape assembly of robot swarms. Nat Commun, 2023, 14: 3476
33 Li J, Ning Z, He S, et al. Three-dimensional bearing-only target following via observability-enhanced helical guidance. IEEE Trans Robot, 2023, 39: 1509–1526
34 Ma X, Jiao Z, Wang Z, et al. 3-D decentralized prioritized motion planning and coordination for high-density operations of micro aerial vehicles. IEEE Trans Control Syst Tech, 2018, 26: 939–953
35 Rubenstein M, Cornejo A, Nagpal R. Programmable self-assembly in a thousand-robot swarm. Science, 2014, 345: 795–799
36 Zhu G L, Liu K X, Gu H B, et al. Neural-network-based fully distributed formation control for nonlinear multi-agent systems with event-triggered communication. Sci China Tech Sci, 2024, 67: 209–220
37 Yuan G S, Duan H B. Extremum seeking control for UAV close formation flight via improved pigeon-inspired optimization. Sci China Tech Sci, 2024, 67: 435–448
38 Beaver L E, Malikopoulos A A. An overview on optimal flocking. Annu Rev Control, 2021, 51: 88–99
39 Fang H, Wei Y, Chen J, et al. Flocking of second-order multiagent systems with connectivity preservation based on algebraic connectivity estimation. IEEE Trans Cybern, 2017, 47: 1067–1077
40 Li X, Zhou R, Sun G, et al. Connectivity-preserving flocking of multiagent systems via selecting critical neighbors. IEEE Trans Network Sci Eng, 2023, 10: 3779–3792
41 Ren W, Atkins E. Distributed multi-vehicle coordinated control via local information exchange. Int J Robust NOnlinear Control, 2007, 17: 1002–1033
42 Zhang X, Jia S, Li X. Improving the synchronization speed of self-propelled particles with restricted vision via randomly changing the line of sight. NOnlinear Dyn, 2017, 90: 43–51
43 Ballerini M, Cabibbo N, Candelier R, et al. Interaction ruling animal collective behavior depends on topological rather than metric distance: Evidence from a field study. Proc Natl Acad Sci USA, 2008, 105: 1232–1237
44 Shah S, Dey D, Lovett C, et al. AirSim: High-fidelity visual and physical simulation for autonomous vehicles. In: Hutter M, Siegwart R (eds.). Field and Service Robotics. Springer Proceedings in Advanced Robotics. Vol. 5. Cham: Springer, 2018. 621–635